energies

MDPI

Article

Computationally Modelling the Use of Nanotechnology to Enhance the Performance of Thermoelectric Materials

Peter Spriggs and Qing Wang *

Department of Engineering, Durham University, Durham DH1 3LE, UK; peter.g.spriggs@durham.ac.uk
* Correspondence: qing.wang@durham.ac.uk; Tel.: +44-191-3342381; Fax: +44-191-3342408

Received: 26 August 2020; Accepted: 25 September 2020; Published: 30 September 2020

Abstract: The increased focus on global climate change has meant that the thermoelectric market has received considerably more attention. There are many processes producing large amounts of waste heat that can be utilised to generate electrical energy. Thermoelectric devices have long suffered with low efficiencies, but this can be addressed in principle by improving the performance of the thermoelectric materials these devices are manufactured with. This paper investigates the thermoelectric performance of market standard thermoelectric materials before analysing how this performance can be improved through the adoption of various nanotechnology techniques. This analysis is carried out through the computational simulation of the materials over low-, mid- and high-temperature ranges. In the low-temperature range, through the use of nanopores and full frequency phonon scattering, $Mg_{0.97}Zn_{0.03}Ag_{0.9}Sb_{0.95}$ performed best with a *ZT* value of 1.45 at 433 K. Across the mid-temperature range a potentially industry leading *ZT* value of 2.08 was reached by $AgSbTe_{1.85}Se_{0.15}$. This was carried out by simulating the effect of band engineering and the introduction of dense stacking faults due to the addition of Se into $AgSbTe_2$. $AgSbTe_{1.85}Se_{0.15}$ cannot be implemented in devices operating above 673 K because it degrades too quickly. Therefore, for the top 200 K of the mid-temperature range a $PbBi_{0.002}Te$–15% Ag_2Te nanocomposite performed best with a maximum *ZT* of 2.04 at 753 K and maximum efficiency of 23.27 at 813 K. In the high-temperature range, through the doping of hafnium (Hf) the nanostructured $FeNb_{0.88}Hf_{0.12}Sb$ recorded the highest *ZT* value of 1.49 at 1273 K. This was closely followed by $Fe_{1.05}Nb_{0.75}Ti_{0.25}Sb$, which recorded a *ZT* value of 1.31 at 1133 K. This makes $Fe_{1.05}Nb_{0.75}Ti_{0.25}Sb$ an attractive substitute for $FeNb_{0.88}Hf_{0.12}Sb$ due to the much lower cost and far greater abundance of titanium (Ti) compared with hafnium.

Keywords: COMSOL; Seebeck coefficient; thermoelectric effect; *ZT*

1. Introduction

1.1. Relevance of Thermoelectric Generators

Thermoelectric generators (TEGs) are devices that turn waste heat energy into electrical energy [1,2]. With half the energy in natural gas and two thirds of the energy in nuclear, coal and many automotive engines being lost as waste heat, it is clear that maximising the amount of this energy that is utilised will help to reduce the strain on the environment caused by these and many other similar processes [3]. Evidence that 64% of the UK public are now worried by the effect humans' actions are having on the climate highlights the increase in focus on environmental issues in recent times [4,5]. As a result, there has been a significant increase in the attention the thermoelectric sector has received. Although thermoelectric devices have often struggled to gain traction in many markets due to their relatively low efficiencies (less than 10%), improving technologies mean these efficiencies are increasing [6]. One particular area of interest in recent times has been the effect nanotechnology can have in altering the

thermoelectric properties and consequently improving the thermoelectric performance of devices [7,8]. By coupling this increase in efficiency with other advantages of TEGs, such as their high reliability, minimal maintenance requirements and ability to be applied to existing hardware, they are becoming a much more desirable prospect. These developments are therefore forecast to cause growth in the thermoelectric market from $300 M in 2018 to an estimated $1.5 Bn by 2028 [9].

1.2. Application of Thermoelectric Generators

As stated by Robert Freer and Anthony V. Powell, almost 71% of greenhouse gas emissions come from power generation (37%), manufacturing industries (17%) and transport (17%) [9]. Consequently, these sectors offer an opportunity for thermoelectric generators to be implemented.

There are large amounts of waste heat that could be exploited from furnaces, incinerators and processes that produce high-temperature exhaust gases [10]. For example, TEGs are being developed to use on gas turbines, steel boilers and automotive exhausts, leading to greater efficiencies and therefore reducing environmental damage caused by these processes [11].

As well as in power generation [12], transport and manufacturing systems, TEGs have applications in wireless sensing, aerospace and wearable devices. The main problem with wireless sensing networks has always been that they have a short battery life. Recent developments have meant that the power consumed by these networks is now in the order of μW, consequently meaning TEGs are a viable option to significantly enhance battery life and eventually remove the need for batteries entirely. One potential application is to utilise waste heat from hot water pipes within buildings to power wireless sensing systems used to control the building environment, such as air temperature and humidity [9].

The concept behind wearable TEGs is that they will use body heat to power the device. Carbon-based nanomaterials are being investigated in this area alongside PEDOT: PSS (poly(3,4-ethylenedioxythiophene) polystyrene sulfonate). Both are desirable as they are organic, low cost and mechanically flexible [9]. In satellites, TEGs take advantage of the heat flows that occur due to environmental and operational heat loads [13]. The fact that TEGs have a solid-state behaviour makes them ideal for satellites, as they do not cause any unwanted vibrations as well as being very reliable and maintenance free. Fundamentally, anywhere a temperature gradient exists there is potential for a TEG to be utilised to generate electrical energy.

1.3. Thermoelectric Material Development

A TEG is formed out of numerous legs, which run electrically in series and thermally in parallel between a temperature gradient. The factor that has the greatest effect on performance is the materials used for these legs of the thermoelectric generator. Consequently, much of the research that is undertaken and investment in the industry focuses on improving the performance of these materials. For the most part, the performance of these materials is evaluated using a dimensionless figure of merit, ZT. In recent times, bismuth telluride has been extensively used for low-temperature thermoelectric applications. The bismuth telluride used in current devices has a ZT value of just below 1 for room temperature applications [14]. Due to its high level of performance it still receives a huge amount of attention within the industry, but tellurium's lack of abundance has led to the potential for a much broader range of materials to be analysed. Magnesium (Mg) is highly abundant, environmentally benign and mechanically flexible, making it desirable for several applications. Consequently, magnesium-based materials were modelled in this investigation across the low- and mid-temperature ranges.

When it comes to mid-range materials, many group-VI tellurides and some antimonides are popular. Some examples of these are GeTe, PbTe, $CoSb_3$ [15] and Mg_3Sb_2. These materials are often alloyed with other materials to enhance their performance. For example, single phase PbTe, used in numerous devices since 1960, has a figure of merit of 0.8, but when Sodium (Na) is added to the material a ZT value of 1.4 is recorded [16]. At high temperatures, SiGe is extensively used due to its inherently low thermal conductivity. Overall, the ZT values recorded at high temperatures are

significantly lower than those achieved at lower temperatures. Even new and more complex materials that have entered the market, such as $Yb_{14}MnSb_{11}$, can only achieve maximum values of 0.7 [17].

Other areas of the thermoelectric market where there have been significant recent advancements are the organic materials and thin film sectors. Some thin film devices have shown improved power factors and have been able to simplify the synthesis process leading to lower costs of production [18]. Organic materials' main advantages are their abundance, low cost and low thermal conductivity and solubility, which means they can be constructed using scalable printing processes [9]. Currently though, the greatest ZT value achieved by organic materials is 0.4, and thin-film TEGs can only be used for niche applications because parts of their geometries, such as the contacts to the metal connections, need to be optimised before they can be used more widely [9].

For these reasons, thin-film generators and organic materials are not evaluated here. The focus of this paper remains on bulk inorganic thermoelectric materials, which are the most broadly used materials across the market.

In this paper, the material selection aspect of designing a TEG was analysed. Materials commonly used across the thermoelectric market, referred to as market standard materials, were simulated across low-, mid- and high-temperature ranges using COMSOL Multiphysics computational modelling software. Potential enhancements to these materials, made possible by the development of various nanotechnologies, were simulated and the effect on thermoelectric performance was analysed.

2. Thermoelectric Theory

2.1. Thermoelectricity

Thermoelectricity is defined as when a difference in temperature is used to develop electrical energy, or the other way around [1]. Throughout a wide range of industries and applications, engineers are using this thermoelectric effect to either produce electricity, calculate temperature, or heat and cool [1]. There are phenomena that are used to do this; the Seebeck effect is used in generating electricity and the Peltier effect is used to heat or cool.

2.2. The Seebeck Effect

When a temperature gradient is applied, this causes the majority carrier in the material—electrons in n-type semiconductors and holes in p-type semiconductors—to move from the warmer, higher energy side to the cooler, lower energy side. This means that a charge gradient is formed between the two sides, which in turn produces a potential difference that will cause a current to flow if connected into a circuit. This process is called the Seebeck effect, which is illustrated in Figure 1, and the potential difference produced is named the Seebeck voltage.

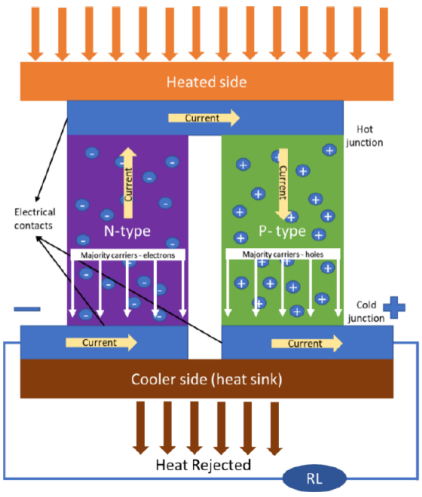

Figure 1. The Seebeck effect.

To model the Seebeck effect, the Seebeck coefficient S is used:

$$S = \frac{\Delta V}{\Delta T} \quad (1)$$

where ΔV is the potential difference between the two terminals, labelled + and − in Figure 1, and ΔT is the difference in temperature between the two sides. Coefficient S is used to illustrate the thermopower of a given material. Metals tend to perform poorly when it comes to thermopower, as generally they have half-filled valence bands, meaning the induced movement of holes and electrons tends to cancel each other out. Doped semiconductors have high thermopowers, as they have large numbers of extra holes or electrons depending on whether they are p-type or n-type. When designing TEGs, the larger the value of S the more desirable the material because the ability to produce a greater induced voltage from a certain temperature difference is what underpins achieving greater efficiencies.

2.3. The Thermoelectric Generator

TEGs are formed out of thermoelectric modules, with each module having an arrangement of p-type and n-type semiconductor legs between the temperature gradient, which can be seen in Figure 2. The main element affecting how well TEGs perform is the materials used within them. Other factors that also contribute are the device architecture, the module geometry, the electrically insulating substrate selected and the thermal and electrical contacts used [19,20].

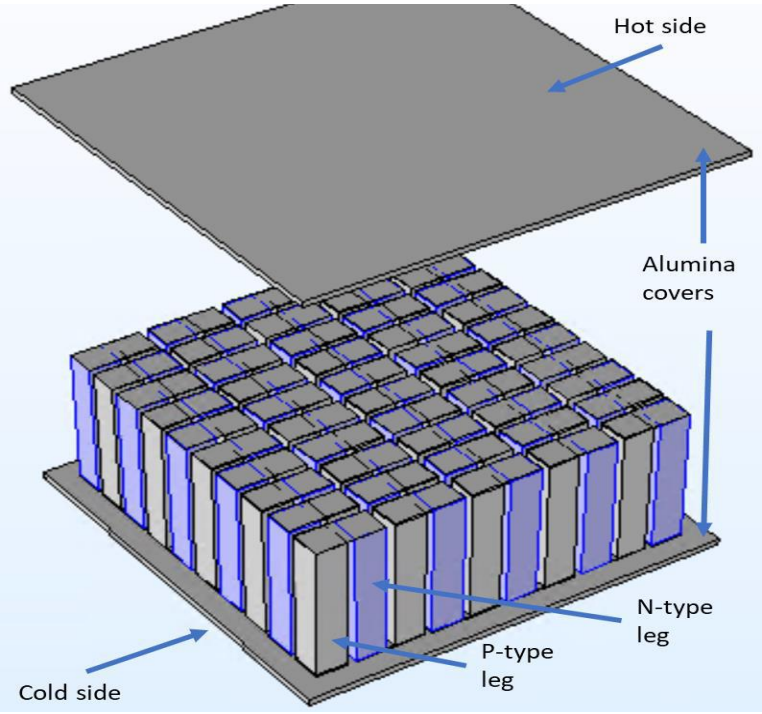

Figure 2. Design of a standard thermoelectric module. The top cover is exploded out to give a clear view of the makeup of the module. In reality, it would sit directly above the legs, just as the bottom plate sits directly below them.

2.4. Modelling Thermoelectric Materials

The performance of a material is given through a figure of merit value, ZT :

$$ZT = \frac{S^2 \sigma T}{k} \quad (2)$$

where S is the Seebeck Coefficient, σ is the electrical conductivity, k is the thermal conductivity, T is the temperature (K) and ZT is the dimensionless figure of merit. The thermal conductivity is formed from contributions from charge carriers, k_e, and lattice vibrations, k_L.

$$k = k_e + k_L \tag{3}$$

In literature, Equation (2) is often amalgamated into a singular parameter, as shown in Equation (4).

$$ZT = \frac{PF}{k} T \tag{4}$$

where PF is the power factor, which is formed from the Seebeck coefficient and electrical conductivity [21]. The power factor can be calculated as

$$PF = S^2\sigma \tag{5}$$

To achieve a high value of ZT and therefore maximise performance, a high Seebeck coefficient and high electrical conductivity are needed alongside a low thermal conductivity. The problem is that materials with a high Seebeck coefficient and low thermal conductivity tend to be non-metallic whereas materials with a high electrical conductivity tend to be metallic. Usually, the most attractive compromise comes in the form of semiconductors that possess charge carrier densities between 10^{19} cm^{-3} and 10^{20} cm^{-3} [9].

Improving figure of merit values is challenging. A rise in temperature increases the energy of the majority carriers, which are electrons in n-type materials and holes in p-type materials. This rise in temperature would therefore be expected to lead to a higher majority carrier concentration. It has been found experimentally though that the Seebeck coefficient is inversely proportional to the carrier concentration because a rise in the majority carrier concentration is accompanied by a rise in the minority carrier concentration. These minority carriers have the opposite effect to the majority carriers and therefore reduce the Seebeck coefficient. This phenomenon is called the bipolar effect [22]. The bipolar effect further leads to reductions in the ZT value a material can achieve by increasing the thermal conductivity. When the total number of carriers, both minority and majority, diffusing across the temperature gradient increases this leads to more heat being transferred from the warmer side to the cooler side, thus causing an increase in thermal conductivity. Materials that have a narrow band gap are affected by the bipolar effect to a greater extent because it is easier for the minority carriers to enter an excited state [6].

By using Equation (2) to calculate the figure of merit for the materials within a thermoelectric device and using the temperature of the hotter surface, T_H, and colder surface, T_C, the efficiency of a material in converting heat energy into electrical energy can be calculated using Equation (6) [6].

$$\eta = \frac{T_H - T_C}{T_H}\left[\frac{\sqrt{1+ZT}-1}{\sqrt{1+ZT}+\frac{T_C}{T_H}}\right] \tag{6}$$

In Equation (2), the Seebeck coefficient, electrical conductivity and thermal conductivity are presented as independent of temperature. In practice, though, this is not the case and all three often change considerably as the temperature is altered. In this investigation, the results from the materials simulated in COMSOL are temperature dependent. Consequently, Equation (2) becomes

$$ZT = \frac{S(T)^2\sigma\,(T)T(T)}{k(T)} \tag{7}$$

By integrating temperature-dependent thermoelectric properties into the models, it is possible to produce much more reliable figure of merit values for the materials simulated.

3. Material Testing Method

3.1. Material to Be Tested

The testing of the materials was split into three temperature ranges. A low-temperature range from 273 K to 473 K, a mid-temperature range from 273 K to 873 K and a high-temperature range from 273 K to 1273 K. These ranges were chosen as they mimic how the low-, mid- and high-temperature ranges are most often defined across the literature. The information amalgamated on applications of thermoelectric generators over these three temperature ranges can be seen in Table 1.

Table 1. Possible thermoelectric generator (TEG) applications, mild and high temperature range applications adopted from Ovik et al. 2016 [23].

Application	Temperature Range, K
Wireless sensor networks	Low, 273–373
Wearable devices	Low, 273–323
IoT applications	Low, 273–323
Geothermal Power Generation	Low, 273–473
Steam Boiler Exhaust	Mid, 503–753
Drying and Baking Ovens	Mid, 503–873
Reciprocating Engine Exhaust	Mid, 503–873
Gas Turbine Exhaust	Mid, 643–813
Annealing Furnace Cooling System	Mid, 698–873
Catalytic Crackers	Mid, 698–873
Heat Transfer Furnaces	Mid, 698–873
Cement Kiln	High, 893–1033
Open Hearth Furnace	High, 923–973
Hydrogen Plants	High, 923–1273
Solid Waste Incinerators	High, 923–1273
Aluminium Refining Furnace	High, 923–1033
Copper Refining Furnace	High, 1033–1085

Analysis of the thermoelectric market shows that there are some materials that are used extensively. These market standard materials are highlighted with bold font in Table 2 and were tested in the first part of the investigation over the three temperature ranges. Potential enhancements of these market standard materials were then simulated through a variety of nanotechnology techniques in COMSOL. These are also listed in Table 2, which therefore shows the entire range of materials computationally modelled in this investigation.

Table 2. The materials tested throughout the course of the investigation.

Material-Chemical Formula	Tested Temperature Range	Material-Chemical Formula	Tested Temperature Range
Bi_2Te_3	Low	$Mg_{2.9875}Na_{0.0125}\ Sb_2$	Mid
$Zn_{0.015}Bi_{0.46}Sb_{1.54}Te_{3.015}$	Low	$CoSb_3$	Mid
YbSi2	Low	$Fe_{0.25}Co_{0.75}\ Sb_{2.965}\ Se_{0.035}$	Mid
YbGe2	Low	PbTe	Mid

Table 2. *Cont.*

Material-Chemical Formula	Tested Temperature Range	Material-Chemical Formula	Tested Temperature Range
$Yb(Si_{0.5}Ge_{0.5})_2$	Low	$PbBi_{0.002}Te$–15%Ag_2Te	Mid
AgSbTe2	Low, Mid	PbTe/7% PbTe@C:Ag	Mid
$AgSbTe_{1.85}Se_{0.15}$	Low, Mid	GeTe	Mid
Mg_2Si	Mid	$Ge_{0.9}Ga_{0.02}$ $Sb_{0.05}Te$	Mid
Mg_2Sn	Mid	PbSe	Mid
$Mg_2Si_{0.3}Sn_{0.7}$	Low	$PbCu_{0.00375}Se$	Mid
$Mg_{1.98}Cr_{0.02}(Si_{0.3}Sn0.7)_{0.98}Bi_{0.02}$	Low, Mid	SiGe	High
MgAgSb	Low, Mid	SiGe- 20% SiMo	High
MgAgSb- 3 at% SnTe	Low, Mid	FeNbSb	High
MgAgSb + CNT	Low, Mid	$Fe_{1.05}$ $Nb_{0.75}Ti_{0.25}Sb$	High
$Mg_{0.97}Zn_{0.03}$ $Ag_{0.9}$ $Sb_{0.95}$	Low, Mid	$FeNb_{0.88}Hf_{0.12}Sb$	High
$Mg_{0.995}$ $Yb_{0.005}Ag_{0.97}Sb_{0.99}$	Low, Mid	$Yb_{14}ZnSb_{11}$	High
Mg_3Sb	Mid	$Yb_{13.5}La_{0.5}Zn$ Sb_{11}	High
$Mg_3Sb_{1.8}Bi_{0.2}$/GNS(80:1)	Mid	$Yb_{14}MnSb_{11}$	High
$Mg_{2.69}Li_{0.01}Cd_{0.5}Sb_2$	Mid	$Yb_{13.82}$ $Pr_{0.18}MnSb_{11}$	High

3.2. Formulating Temperature-Dependent Models

COMSOL Multiphysics, with the Heat Module add-on, was chosen to run the temperature-dependent thermoelectric simulations [24]. The geometry of a single thermoelectric leg was constructed with copper plates attached to either end, shown in Figure 3a. The dimensions of the leg and plates respectively were 2 mm × 2 mm × 10 mm and 2 mm × 2 mm × 0.1 mm.

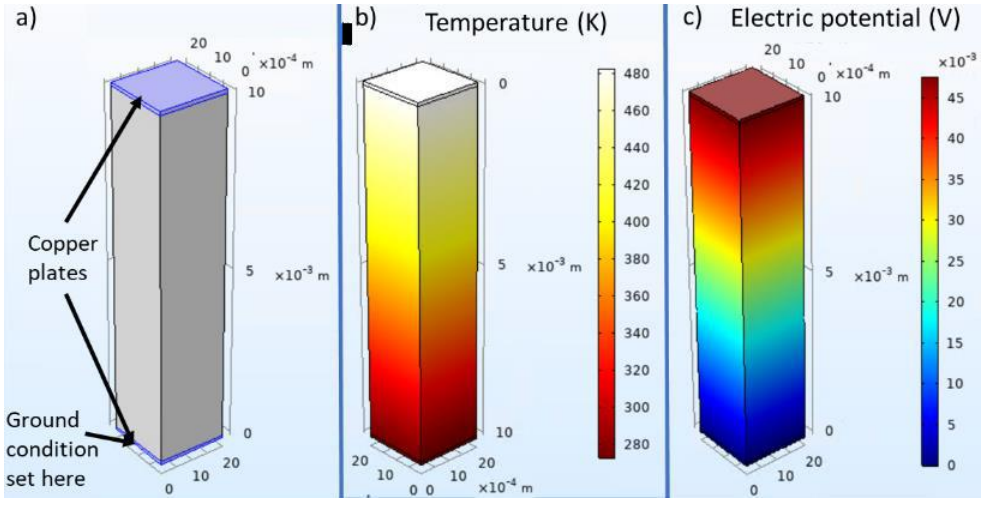

Figure 3. Single thermoelectric leg constructed on COMSOL displaying (**a**) dimensions, (**b**) temperature gradient, (**c**) electric potential.

Once the geometry had been created, further conditions were added to the simulation. The 'thermoelectric physics' module was added to the model, with additional 'heat transfer in solids' and 'electric currents' sub-modules applied to the entire model, while the 'thermoelectric effect' sub-module was applied to the leg only. Figure 3b shows the temperature gradient across the leg. The

bottom side was set as the cold side at a temperature of 273 K and this remained constant throughout the investigation. The top side was varied in order to adjust the temperature difference. The material for the plates was copper, an effective conductor of electricity that is often used within TEGs [25]. A ground condition was set on the left-hand face of the bottom copper plate, labelled in Figure 3a. The electric potential generated was then recorded for each material over its corresponding temperature range (example shown in Figure 3c).

4. Results and Discussion

The market standard materials were modelled over each temperature range (low, mid and high), and their performance was evaluated. The impact of nanotechnology techniques was then investigated to see how they can be used to advantageously alter the thermoelectric properties of each material, hence leading to a considerable increase in a material's thermoelectric performance.

4.1. Initial Testing

4.1.1. Testing Market Standard Low-Temperature Materials

Figure 4 shows how each of the market standard materials performed when simulated between 273 K and 473 K.

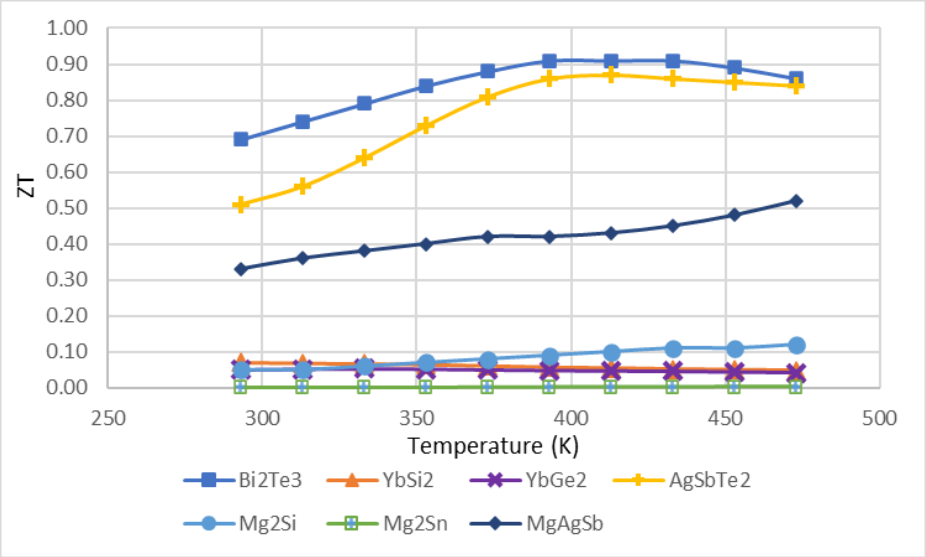

Figure 4. The thermoelectric performance of market standard thermoelectric materials over the low-temperature range: Bi_2Te_3 has the best performance across the entire low-temperature range with a peak *ZT* of 0.91. $AgSbTe_2$ performs comparably, with a peak *ZT* of 0.84 and efficiency of 7.79% at 473 K. There is a sizeable jump down in the performance of MgAgSb. Its *ZT* starts at 0.33 and finishes at 0.52 at 473 K.

Bismuth telluride (Bi_2Te_3) has been at the forefront of the thermoelectric industry and it is shown why here, recording the best performance with a peak *ZT* of 0.91, which is maintained over a 40 K range from 395 K to 435 K [26]. It also maintains an average *ZT* across the entire low-temperature range of 0.84. The efficiency peaks at a value of 7.92% at 473 K. At lower temperatures, from 273 K to 373 K, Bi_2Te_3 considerably outperforms the next best performing material, $AgSbTe_2$, with a difference in *ZT* of 0.18 at 300 K. At the higher end of the temperature range though, $AgSbTe_2$ performs comparably, with a peak *ZT* of 0.84 and efficiency of 7.79% at 473 K [27]. $AgSbTe_2$ performed comparably with the investigation carried out by Hong et al. 2018, where it shows an almost linear increase between 290 K and 390 K and then plateaus [28].

There is a sizeable jump down in the performance of MgAgSb. Its *ZT* starts at 0.33 and finishes at 0.52 at 473 K. Its maximum efficiency over this range is 5.44%, also occurring at 473 K. The remaining materials tested all performed poorly in comparison to the best performing three, with the peak *ZT* recorded between them only 0.12. The *ZT* of Mg_2Sn only reached 0.03 over the temperature range. However, when the metal silicides Mg_2Si and $YbSi_2$ are doped with tin (Sn) and germanium (Ge) respectively, promising thermoelectric materials can be formed, as shown in Figure 5.

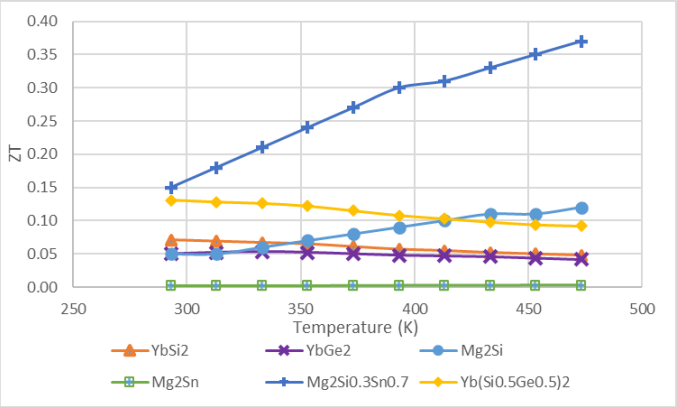

Figure 5. The advances in performance possible for Mg_2Si and $YbSi_2$ when doped with Sn and Ge respectively: at 473 K, the ZT value of $Mg_2Si_{0.3}Sn_{0.7}$ is 0.37, which is over three times greater than that of Mg_2Si. Although $Yb(Si_{0.5}Ge_{0.5})_2$ does perform significantly better than $YbGe_2$ and $YbSi_2$, it proves to be a promising material for thermoelectric performance going forward due to its high power factor at room temperature (3.7 $mWm^{-1}K^{-2}$). Data from [29].

$Mg_2Si_{0.3}Sn_{0.7}$ performs poorly at room temperature with a *ZT* of 0.15, but at 473 K its *ZT* of 0.37 is over three times greater than that of Mg_2Si. It also has a far greater efficiency, which peaks at 4.12% at 473 K, compared with Mg_2Si, which has a peak efficiency of 1.51% occurring at the same temperature. Although the performance of $Yb(Si_{0.5}Ge_{0.5})_2$ does perform significantly better than $YbGe_2$ and $YbSi_2$, it still remains far below the other four materials tested in this temperature range. Even with these low levels of performance $Yb(Si_{0.5}Ge_{0.5})_2$ has received significant amounts of attention recently, with Tanuslip and Kurosaki 2019 finding it to be a promising material for thermoelectric performance going forward due to its high power factor at room temperature (3.7 $mWm^{-1}K^{-2}$) [29]. In addition, silicon-based materials can be utilised commercially much more easily than other thermoelectric materials due to their abundance, inexpensiveness and non-toxicity. The commercial utilisation of materials and the journey from the laboratory to the market has long been a problem for the industry, so materials that make this path easier are highly desirable. However, as the magnesium silicide performs significantly better than the ytterbium, no further testing was done on $Yb(Si_{0.5}Ge_{0.5})_2$ and an enhancement of $Mg_2Si_{0.3}Sn_{0.7}$ was chosen to be modelled in part 2 of the results due to its superior performance.

4.1.2. Testing Market Standard Mid-Temperature Materials

Figure 6 shows the performance of the materials tested across the mid-temperature range, between 273 K and 873 K.

The best performing material in this range was $AgSbTe_2$ with a peak *ZT* of 1.3 and efficiency of 15.97% at 673 K. This is marginally higher than the peak *ZT* of PbTe of 1.28 at 873 K. However, the peak efficiency of PbTe is the greatest of any of the materials across this range with a value of 19.22% at 873 K. For $AgSbTe_2$, the thermal conductivity and electrical conductivity behave in similar ways from 273 K to 673 K, consequently cancelling each other's effect and there being little effect on *ZT*. They both decrease markedly between 273 K and 500 K before then increasing slightly from 500 K to 673 K. The Seebeck coefficient varies considerably too, increasing until 400 K, causing a steep rise

in *ZT*. It then decreases until 520 K, causing a slight decrease in *ZT*. As can be seen in Equation (2), increasing temperature causes an increase in *ZT*, therefore the reduction in *ZT* caused by the decrease in S is minimised by the increasing temperature. Between 500 K and 673 K, S then starts to increase again leading to another rise in *ZT* up until its peak of 1.3 at 673 K.

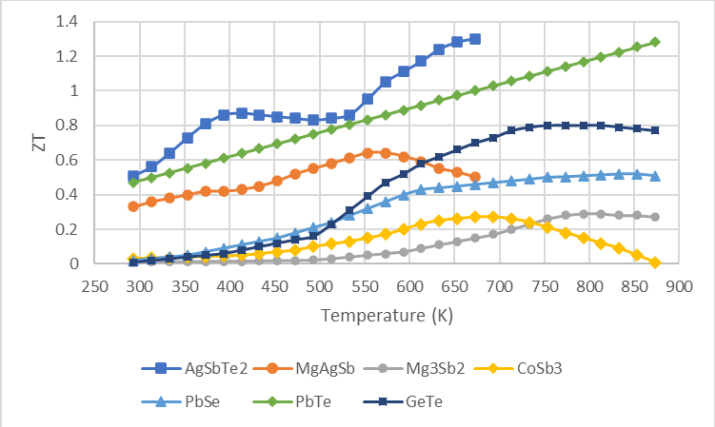

Figure 6. The thermoelectric performance of market standard thermoelectric materials over the mid-temperature range: $AgSbTe_2$ records the highest *ZT* value, and the peak efficiency of the PbTe is greatest of any of the materials across this range with a value of 19.22% at 873 K. MgAgSb has three different phase structures, α-MgAgSb, β-MgAgSb and γ-MgAgSb. Due to the twisted half-Heusler structure of α-MgAgSb, it has better thermoelectric properties, especially across the low- and mid-temperature ranges investigated here. The *ZT* value of GeTe increases at a much greater rate from 500 K and remains similar from 700 K onwards.

Although $AgSbTe_2$ records the highest *ZT* value, the peak efficiency of PbTe is the greatest of any of the materials across this range with a value of 19.22% at 873 K. PbTe behaves very close to linearly over the temperature range as over this range the Seebeck coefficient, thermal conductivity and electrical conductivity all remain at very similar levels, thus, *ZT* increases as the temperature climbs.

For MgAgSb, the electrical conductivity, thermal conductivity and the Seebeck coefficient all remain at similar values between 273 K and 550 K, leading to a close to linear increase in the *ZT* as the temperature rises. However, once past 550 K the Seebeck coefficient starts to fall, which leads to a reduction in the *ZT* value. The same material with differing phase structures can have starkly different thermoelectric properties. This is particularly true for MgAgSb, which has three different phase structures, α-MgAgSb, β-MgAgSb and γ-MgAgSb. Due to the twisted half-Heusler structure of α-MgAgSb, it has better thermoelectric properties, especially across the low- and mid-temperature ranges investigated here [30]. Consequently, the MgAgSb and the relative enhancements investigated here are all of the α-MgAgSb phase structure.

Both $AgSbTe_2$ and MgAgSb are designed as low-mid-range materials. Both materials start to degrade quickly when forced to operate above 673 K, thus meaning they are no longer viable options for thermoelectric applications at these temperatures. Consequently, they were not modelled above 673 K.

For most materials evaluated here, as the temperature increases the thermal conductivity and electrical conductivity decreases. By referencing Equation (2), it can be seen that a decreasing thermal conductivity will increase the *ZT*, whereas a decreasing electrical conductivity will have the opposite effect. The aim therefore is to decrease electrical conductivity as slowly as possible while decreasing thermal conductivity as quickly as possible. Many of these mid-range materials demonstrate subjectively low electrical conductivity, low Seebeck coefficient and high thermal conductivity until around the 500 K mark.

For GeTe, from 273 K to 500 K the electrical conductivity falls significantly from 70,000 S/m to 32,000 S/m. Between 500 K and 873 K, though, the drop is only 13,000 S/m, taking the electrical

conductivity to 19,000 S/m. Meanwhile, according to Srinivasan et al. between 273 K and 700 K the thermal conductivity drops from 6.7 $Wm^{-1}K^{-1}$ to 2.8 $Wm^{-1}K^{-1}$ at a constant rate [31]. Therefore, when the electrical conductivity plateaus at 500 K the *ZT* value starts to increase as the thermal conductivity continues to decrease. This is what causes the *ZT* value of GeTe to increase at a much greater rate from 500 K. The *ZT* level then remains similar from 700 K onwards, as at this point the thermal conductivity starts decreasing at a considerably slower rate and the Seebeck coefficient reaches its maximum value of 140 μVK^{-1} and plateaus.

4.1.3. Testing Market Standard High-Temperature Materials

There are a range of applications, such as steel, zinc and copper furnaces, as well as incinerators and hydrogen plants, where there is an opportunity for TEGs to be implemented in order to convert the waste heat energy produced by these processes into useful electrical energy, consequently markedly increasing the efficiency of these processes. Figure 7 shows the materials analysed using COMSOL over the high-temperature range.

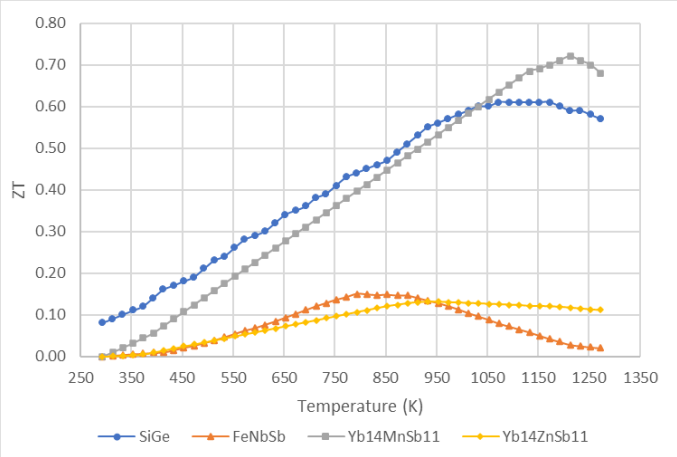

Figure 7. The thermoelectric performance of market standard thermoelectric materials over the high-temperature range: $Yb_{14}MnSb_{11}$ records a *ZT* value of 0.72 at 1193 K and an efficiency of 15.66% at 1233 K. Silicon-germanium (SiGe) is the next best performing material, with a peak *ZT* of 0.61 that is maintained from 1073 K to 1173 K and a peak efficiency of 13.70% at 1233 K. Neither $Yb_{14}ZnSb_{11}$ nor FeNbSb record a *ZT* value over 0.15 but FeNbSb behaves like the majority of half-Heusler structures with a high power factor, reaching 5 $mWm^{-1}K^{-2}$.

$Yb_{14}MnSb_{11}$ records a *ZT* value of 0.72 at 1193 K and an efficiency of 15.66% at 1233 K. Both are the peak values for any of the four materials across the temperature range. There is a reduction in the Seebeck coefficient as the temperature increases above 1200 K, leading to a corresponding dip in the *ZT* values. Silicon-germanium (SiGe) is the next best performing material, with a peak *ZT* of 0.61 that is maintained from 1073 K to 1173 K and a peak efficiency of 13.70% at 1233 K. The potential for SiGe as a high-temperature material is clear from these results as it maintains a *ZT* of 0.5 or greater from 873 K to 1273 K. Neither $Yb_{14}ZnSb_{11}$ nor FeNbSb record a *ZT* value over 0.15. FeNbSb behaves like the majority of half-Heuslers with a high power factor, reaching 5 $mWm^{-1}K^{-2}$, but also with a high thermal conductivity due to high k_L values. Without adjustments being made to the material the thermal conductivity is too high to record any *ZT* values of note, whereas $Yb_{14}ZnSb_{11}$ requires a boost in the Seebeck coefficient to record higher *ZT* values across the temperature range.

4.2. Enhancing Thermoelectric Materials through the Use of Nanotechnology

In recent years, there has been a significant drive within the thermoelectric market to use nanotechnology to advantageously alter thermoelectric characteristics and increase *ZT* values of materials. Each material modelled is enhanced through the use of nanotechnology in at least one way.

At the low-temperature range, enhancements of the magnesium-based materials are tested, while enhancements of Bi_2Te_3 [32–34] and $AgSbTe_2$ are also investigated to provide a reference point for performance. The effects of various techniques were simulated: the use of nanopores, doping, nanostructuring and the formation of nanoprecipitates. In the mid-temperature range, the magnesium-based materials did not perform as well; therefore, enhancements of the other materials came to the fore. The techniques simulated here were phonon scattering, the introduction of dense stacking faults, forming nanocomposites and nanoprecipitates, the insertion of carbon nanotubes, nanoinclusions and the use of graphene nanosheets. Over the high-temperature range, most of the enhancements are carried out through doping. The effect of reducing grain size was also investigated when simulating the performance of $Fe_{1.05}Nb_{0.75}Ti_{0.25}Sb$.

4.2.1. Enhanced Low-Temperature Thermoelectric Materials

One of the main challenges of the thermoelectric industry is getting the materials developed in the laboratory to the market. Key factors affecting this are that many of the materials used are often rare, high cost and are themselves environmentally damaging. Consequently, in this section there has been a focus on making enhancements to the magnesium-based materials tested, as magnesium is low cost, environmentally benign and its abundance is significantly greater than that of tellurium, a core ingredient in the widely-used bismuth telluride [35–38]. Enhancements of Bi_2Te_3 and $AgSbTe_2$ were also modelled here, to see how the new developments in magnesium-based thermoelectric materials compare against other state-of-the-art thermoelectric materials. Figure 8 shows the enhanced low-temperature materials.

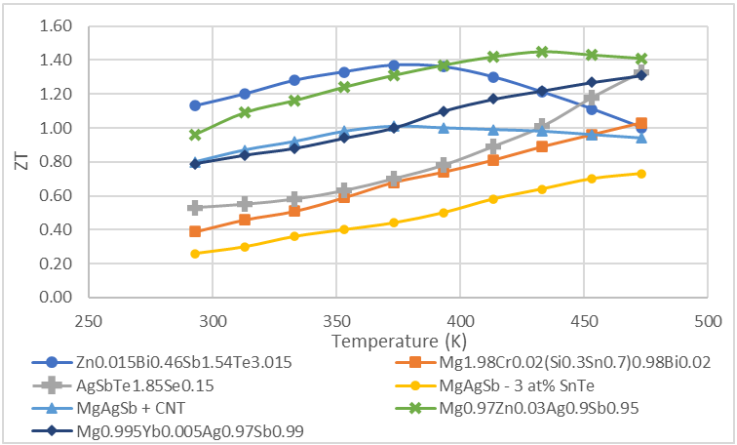

Figure 8. The thermoelectric performance of market standard thermoelectric materials over the high-temperature range: $Mg_{0.97}Zn_{0.03}Ag_{0.9}Sb_{0.95}$ has an average *ZT* value of 1.28 across the 200 K low-Table 0. $Bi_{0.46}Sb_{1.54}Te_{3.015}$ gives an average *ZT* value across the temperature range of 1.23, peaking at a value of 1.37 at 373 K. By using a melt-spinning-based synthesis during the production of the material, nanostructuring could take place that allows zinc telluride nanoprecipitates to form within the material.

$Mg_{0.97}Zn_{0.03}Ag_{0.9}Sb_{0.95}$ records the greatest *ZT* value of 1.45 at 433 K and has the greatest efficiency of 10.96% at 473 K. These COMSOL results are comparable to those shown by Yu et al. (2020), who found a similar maximum *ZT* of 1.40 at 423 K [39]. Another key aspect to highlight is the average *ZT* value over the entire temperature range. $Mg_{0.97}Zn_{0.03}Ag_{0.9}Sb_{0.95}$ has an average *ZT* value of 1.28 across the 200 K low-temperature range, which exemplifies the appeal of this material

at these temperatures. These high ZT values are possible because the thermal conductivity has been significantly reduced through a variety of nanotechnology techniques.

As indicated in Equation (3), thermal conductivity is the sum of lattice vibrations (k_L) and contributions from charge carriers (k_e). The lattice vibrations can be significantly reduced by using full frequency phonon scattering. In order to implement such broad frequency phonon scattering, two techniques are implemented: nanopores are utilised and zinc doping is carried out at the magnesium sites. Consequently, with these techniques Zheng et al. (2019) were able to achieve an ultra-low k_L value of 0.45 $Wm^{-1}K^{-1}$ [40]. Alongside the reduction in k_L, recent discoveries by Zheng et al. have also meant that the electrical conductivity can be increased through the enhancement of the carrier concentration and mobility. This can be achieved through the further use of zinc doping and by heat-treating the material over the course of a ten-day period [22].

The next best performing material across the range was the enhanced bismuth telluride, $Zn_{0.015}Bi_{0.46}Sb_{1.54}Te_{3.015}$. From the COMSOL simulations, it gives an average ZT value across the temperature range of 1.23, peaking at a value of 1.37 at 373 K. This maximum ZT value is just under that recorded by Deng et al. (2018), who found that by using a melt-spinning-based synthesis during the production of the material, nanostructuring could take place that allows zinc telluride nanoprecipitates to form within the material [26]. The effect of this is to give very low lattice vibrations, meaning a k_L of below 0.6 $Wm^{-1}K^{-1}$ is recorded from 273 K to 373 K, before it increases up to 0.8 $Wm^{-1}K^{-1}$ at 473 K.

As can be seen from Figure 8, $Zn_{0.015}Bi_{0.46}Sb_{1.54}Te_{3.015}$ performs better across the first 120 K of the 200 K range than $Mg_{0.97}Zn_{0.03}Ag_{0.9}$ $Sb_{0.95}$. This suggests that it is a favourable material for near room temperature applications. For example, wearables that use the human body to create a temperature difference and produce electrical power do not need to operate at temperatures over 323 K. Therefore, if looking at performance alone, $Zn_{0.015}Bi_{0.46}Sb_{1.54}Te_{3.015}$ would be the most appropriate material for this application. However, most wearable microelectronics have low power requirements of around 70 µW [9]. This reduces the importance of picking the best performing material, as numerous materials can achieve this. Other important factors, such as abundance, cost and mechanical flexibility of the material will have more influence on commercial decision-making.

The techniques of full frequency phonon scattering, zinc nanostructuring and the use of nanopores have given an abundant, environmentally benign and mechanically strong material, $Mg_{0.97}Zn_{0.03}Ag_{0.9}$ $Sb_{0.95}$, the potential to lead the way in the low-temperature thermoelectric material market. The low cost and abundance of the material should also mean that the path from laboratory testing to production should be quicker and easier than in the past, especially due to the far greater investment in the thermoelectric market now being made.

4.2.2. Enhanced Mid-Temperature Thermoelectric Materials

As can be seen in Figure 9, fourteen possible enhancements for the mid-temperature range materials were tested.

$AgSbTe_{1.85}Se_{0.15}$, the enhancement of $AgSbTe_2$, gives the greatest ZT value of 2.08 over this range. This is in keeping with the results from Hong et al. (2018) who also managed to record a ZT value greater than 2 [33]. Here, low k_L values are achieved by introducing dense stacking faults in order to enhance phonon scattering. By using band engineering, the power factor of $AgSbTe_{1.85}Se_{0.15}$ can be increased. By simultaneously increasing the power factor and decreasing the thermal conductivity, potentially industry-leading ZT values can be recorded. The band engineering undertaken includes adding extra valence bands to the material. In the past, this has led to a reduction in carrier mobility, and therefore electrical conductivity, because the introduced bands are heavier than the fundamental ones. However, in $AgSbTe_2$ an extra light valence band exists, which means that multibands can be added without the usual decrease in carrier mobility. Adding more bands to the material reduces the band offset, and the smaller the band offset the better the distribution of the carriers [41]. The addition of selenium here also reduces the band offset between the light valence band and primary valence band, which leads to greater carrier distribution and therefore enhanced electronic transport.

Like $AgSbTe_2$, $AgSbTe_{1.85}Se_{0.15}$ starts to degrade very quickly once it operates above 673 K, so it was only tested up to this temperature.

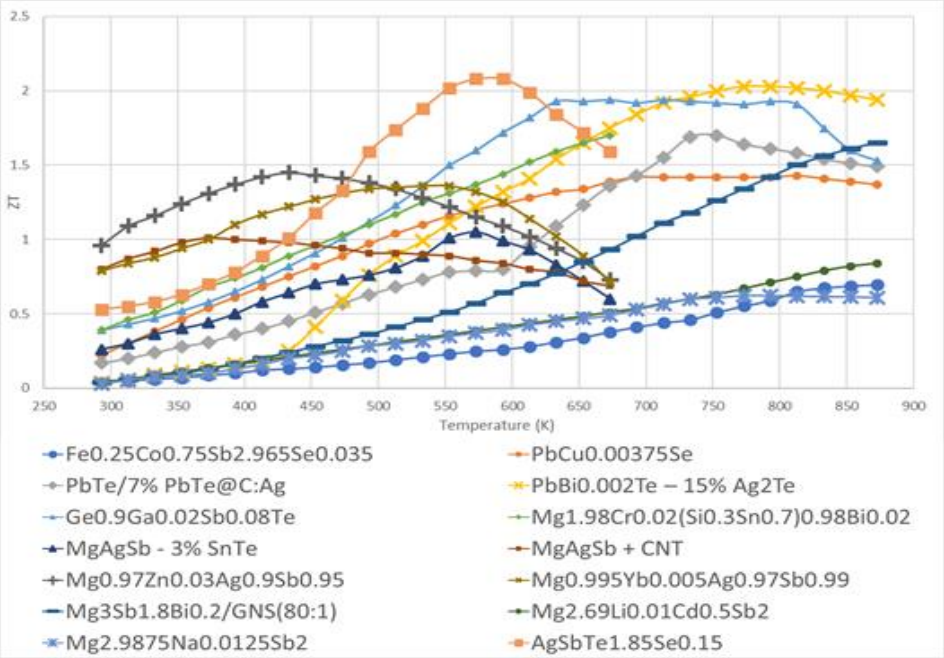

Figure 9. The thermoelectric materials enhanced through a range of nanotechnology techniques across a mid-temperature range: $AgSbTe_{1.85}Se_{0.15}$ gives the greatest *ZT* value of 2.08 over this range, achieved by simultaneously increasing the power factor and decreasing the thermal conductivity. Between 625 K and 873 K, there are two materials that stand out: $Ge_{0.9}Ga_{0.02}Sb_{0.08}Te$ and the Bi-doped PbTe/Ag_2Te nanocomposite. PbTe/7% PbTe@C:Ag was formed by mixing a base of PbTe@C:Ag nanoparticles with PbTe nanocubes, and it performed well but does not have the same performance as $PbBi_{0.002}Te$–15% Ag_2Te, which recorded a *ZT* value of 1.70 at 753 K and a maximum efficiency of 21.00% at 873 K. $Ge_{0.9}Ga_{0.02}Sb_{0.08}Te$, made by hybrid flash-spark plasma sintering, Ga and Sb doping reaches a *ZT* value of 1.91 at 613 K. Three enhancements, MgAgSb with carbon nanotubes inserted, MgAgSb with 3% SnTe nanoinclusions and $Mg_{0.995}Yb_{0.005}Ag_{0.97}Sb_{0.99}$ all had *ZT* values that were increasing at 473 K. $Mg_3Sb_{1.8}Bi_{0.2}$/GNS (80:1) was formed by doping with Bi and then producing an $Mg_3Sb_{1.8}Bi_{0.2}$/graphene nanosheet (GNS) nanocomposite with a mass ratio of 80:1.

Between 625 K and 873 K, there are two materials that stand out; the enhancement of GeTe, $Ge_{0.9}Ga_{0.02}Sb_{0.08}Te$, and one of the enhancements of PbTe, which is the Bi-doped PbTe/Ag_2Te nanocomposite. Lee et al. (2019) theoretically suggested that the nanocomposite consisting of 15% Ag_2Te would perform the best [42]. Therefore, this was the form of the nanocomposite chosen to be computationally modelled using COMSOL. Due to the nanocomposite showing insulating behaviour near room temperature, the electrical conductivity remains close to zero up until around 425 K. From here, it starts to increase, leading to an increase in *ZT*. The reason for this is that Ag_2Te experiences a structural phase transition once the temperature passes 425 K. This change from monoclinic β-Ag_2Te to cubic α-Ag_2Te leads to a sudden increase in both electrical conductivity and Seebeck coefficient while having no noticeable effect on thermal conductivity [39]. PbTe-based materials are narrow band gap semiconductors and so are significantly affected by the bipolar effect, especially at high temperatures. The addition of Ag_2Te helps to mitigate the magnitude of this bipolar effect. This conglomeration of factors means a *ZT* value of 2.04 was recorded at 753 K and a maximum efficiency of 23.27% was recorded at 813 K.

The other enhancement of PbTe modelled was PbTe/7% PbTe@C:Ag. Xiang et al. (2019) developed this material by mixing a base of PbTe@C:Ag nanoparticles with PbTe nanocubes and it performed

well, but it could not match the performance levels reached by its counterpart, $PbBi_{0.002}Te$–15% Ag_2Te, when modelled using COMSOL. It recorded a *ZT* value of 1.70 at 753 K and a maximum efficiency of 21.00% at 873 K.

$Ge_{0.9}Ga_{0.02}Sb_{0.08}Te$ reaches a *ZT* value of 1.91 at 613 K and then remains at a similar value (±0.02) up until 813 K. The maximum efficiency of the material is 22.76% at 813 K. Through the process of hybrid flash-spark plasma sintering, gallium (Ga) and antimony (Sb) doping was completed by Srinivasan et al. (2019), who found a higher peak *ZT* value of 1.95 but exhibited a similar range where a high *ZT* value was maintained between 600 K and 800 K [31]. The way the material maintains its *ZT* value over the 180 K range from 633 K to 813 K makes it an attractive option for waste heat energy conversion for mid-temperature range applications.

The four enhancements of MgAgSb tested across the low-temperature range were also tested across the mid-temperature range. $Mg_{0.97}Zn_{0.03}Ag_{0.9}Sb_{0.95}$ was selected because it recorded a competitive *ZT* value of 1.41 at the high end of the low-temperature range at 473 K. The other three enhancements, MgAgSb with carbon nanotubes (CNT) inserted, MgAgSb with 3% SnTe nanoinclusions and $Mg_{0.995}Yb_{0.005}Ag_{0.97}Sb_{0.99}$, were tested across the mid-temperature range because all had *ZT* values that were increasing at 473 K, as illustrated in Figure 8. However, as shown in Figure 9, after 500 K the *ZT* levels of each of the enhancements decreased markedly, suggesting that the enhancements of MgAgSb tested in this investigation are more suited to the lower temperature range. The reason for this drop in *ZT* is that in all four materials the thermal conductivity starts to increase rapidly from 500 K. This is because at 500 K MgAgSb starts transitioning away from the tetragonal α-MgAgSb into its intermediate tetragonal phase, β-MgAgSb. Then, at 650 K, it transitions into γ-MgAgSb, which has a cubic structure and is a poor thermoelectric material [43]. One reason for this is that it causes a large drop in carrier concentration and therefore electrical conductivity.

$Mg_{1.98}Cr_{0.02}(Si_{0.3}Sn_{0.7})_{0.98}Bi_{0.02}$ recorded a maximum *ZT* value of 1.82 at 673 K, which is higher than any metal silicide thermoelectric material currently being produced. It also recorded an efficiency of 19.36% at 673 K. These results are in line with those of Goyal et al. (2019), who doped $Mg_2Si_{0.3}Sn_{0.7}$ with bismuth (Bi) and chromium (Cr). Goyal et al. found that the Bi increased the electrical conductivity due to band convergence, and introducing Cr caused embedded Cr and Sn nanoprecipitates to form within the material, helping to keep the thermal conductivity as low as possible [44]. The overall result of this nanodoping was to increase the electrical conductivity to 2100 Scm^{-1} at 273 K. From there it decreases to 1400 Scm^{-1} at 673 K. In comparison, undoped $Mg_2Si_{0.3}Sn_{0.7}$ has an electrical conductivity of 100 Scm^{-1} at 273 K, increasing slightly to 200 Scm^{-1} by 673 K. The challenge is to keep thermal conductivity low with such a significant increase in electrical conductivity. This is achieved, as the undoped material has a thermal conductivity of 2.2 $Wm^{-1}K^{-1}$ at 273 K rising to 2.7 $Wm^{-1}K^{-1}$ at 673 K. $Mg_{1.98}Cr_{0.02}(Si_{0.3}Sn_{0.7)0.98}Bi_{\ 0.02}$ has a higher thermal conductivity of 2.7 $Wm^{-1}K^{-1}$ at 273 K, but this reduces to 2.4 $Wm^{-1}K^{-1}$ by 673 K. By maintaining a comparable thermal conductivity to the undoped material, a high *ZT* value for $Mg_{1.98}Cr_{0.02}(Si_{0.3}Sn_{0.7)0.98}Bi_{\ 0.02}$ was realised through the significant increase in electrical conductivity.

$PbCu_{0.00375}Se$, the enhancement of PbSe, performed well, with a maximum figure of merit value of 1.42 maintained over a 120 K range from 693 K to 813 K and a maximum efficiency of 20.01% at 873 K. An always-reducing electrical conductivity and Seebeck coefficient across the temperature range means that when the thermal conductivity stops decreasing at 600 K, remaining at 0.7 $Wm^{-1}K^{-1}$ from 600 K to 873 K, the *ZT* values start to plateau.

Due to the advantages of magnesium mentioned previously, three enhancements of Mg_3Sb_2 were simulated. A promising thermoelectric material can be formed by doping with Bi and then producing a $Mg_3Sb_{1.8}Bi_{0.2}$/graphene nanosheet (GNS) nanocomposite with a mass ratio of 80:1. $Mg_3Sb_{1.8}Bi_{0.2}$/GNS (80:1) was modelled here after an investigation by Bhardwaj et al. (2015) found this material to have a *ZT* of 1.30 at 773 K [45]. The modelling carried out using COMSOL produced a similar *ZT* level of 1.34 at 773 K. However, Bhardwaj et al. (2015) did not test at temperatures above 773 K, and when $Mg_3Sb_{1.8}Bi_{0.2}$/GNS (80:1) was modelled using COMSOL between 773 K and 873 K the maximum *ZT*

value recorded was 1.65 and the maximum efficiency was 22.23%, both at 873 K. $Mg_{2.69}Li_{0.01}Cd_{0.5}Sb_2$ and $Mg_{2.9875}Na_{0.0125}Sb_2$ recorded maximum *ZT* values of 0.84 and 0.62 respectively, meaning they both struggle to compete with their magnesium counterpart $Mg_3Sb_{1.8}Bi_{0.2}$/GNS (80:1). This is because towards the high end of the temperature range $Mg_3Sb_{1.8}Bi_{0.2}$/GNS (80:1) has a low thermal conductivity of 0.4 $Wm^{-1}K^{-1}$ whereas the values for $Mg_{2.9875}Na_{0.0125}Sb_2$ and $Mg_{2.69}Li_{0.01}Cd_{0.5}Sb_2$ are at least double that, at 1.0 $Wm^{-1}K^{-1}$ and 0.8 $Wm^{-1}K^{-1}$, respectively.

The poorest performing material across the majority of the mid-temperature range was the enhancement of $CoSb_3$. Through doping of Fe and Se, $Fe_{0.25}Co_{0.75}Sb_{2.96}5Se_{0.035}$ can be formed and a maximum *ZT* value of 0.67 at 873 K was achieved with a maximum efficiency of 12.86% at the same temperature. It should be noted, however, that through further nanostructuring Bhardwaj et al. (2019) achieved a $ZT > 0.7$ when testing $Fe_{0.25}Co_{0.75}Sb_{2.965}Se_{0.035}$ [46]. Although $Fe_{0.25}Co_{0.75}Sb_{2.965}Se_{0.035}$ does not perform well based on its *ZT* value, it does still have a place in the thermoelectric market. For applications where the speed and cost of production are important, $Fe_{0.25}Co_{0.75}Sb_{2.965}Se_{0.035}$ becomes desirable, as it can be produced through an arc-melting and spark plasma sintering process, which is both fast and easily scalable. An example of a mid-temperature range application where speed and scalability are significant is in the automotive industry, where TEGs can be utilized to take advantage of waste heat in exhaust gases. Due to the maturity of the global car market, reducing lead times and lowering costs are of great value.

4.2.3. Enhanced High-Temperature Thermoelectric Materials

Two enhancements of FeNbSb were modelled for potential use in high-temperature applications alongside one enhancement for each of SiGe, $Yb_{14}MnSb_{11}$ and $Yb_{14}ZnSb_{11}$. The results of the COMSOL modelling over the high-temperature range (273 K–1273 K) are shown in Figure 10.

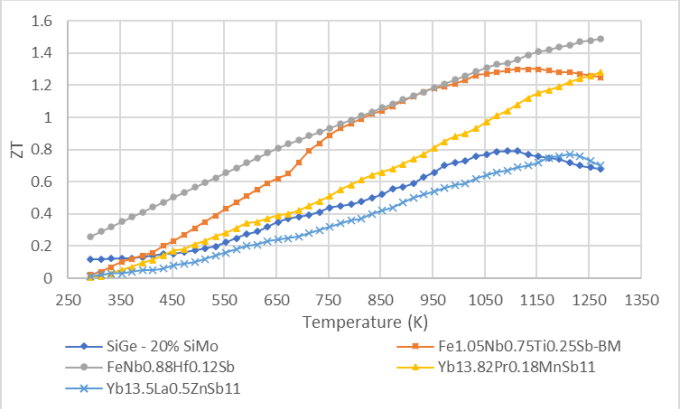

Figure 10. The thermoelectric materials enhanced through a range of nanotechnology techniques across a high-temperature range: $FeNb_{0.88}Hf_{0.12}Sb$ has the highest *ZT*, with a peak value of 1.49 and maximum efficiency of 25.33% at 1273 K. $Fe_{1.05}Nb_{0.75}Ti_{0.25}Sb$ records a maximum *ZT* value of 1.31 at 1133 K and a maximum efficiency of 22.91% at 1273 K. This is achieved by using Ti doping and a ball milling process. $Yb_{13.82}Pr_{0.18}MnSb_{11}$ shows a significant improvement on $Yb_{14}MnSb_{11}$ with a maximum *ZT* of 1.28 and a maximum efficiency of 23.23% at 1273 K. Neither SiGe—20% SiMo nor $Yb_{13.5}La_{0.5}ZnSb_{11}$ manage to achieve *ZT* values above 0.9, with maximum values of 0.88 at 1273 K and 0.77 at 1213 K, respectively. Such a dramatic rise in *ZT* from $Yb_{14}ZnSb_{11}$ to $Yb_{13.5}La_{0.5}ZnSb_{11}$ is surprising considering the La^{3+} ions are simply replacing the Yb^{3+} ions in the material and therefore would not be expected to drastically affect *ZT*.

The main focus of this graph is the temperature range between 873 K and 1273 K, as below 873 K there are no figure of merit values above 1.2. Therefore, the materials do not compete over the low- and mid-temperature ranges. Between 873 K and 1273 K, $FeNb_{0.88}Hf_{0.12}Sb$ has the highest *ZT*, with a peak value of 1.49 and maximum efficiency of 25.33% at 1273 K. From 300 K to 900 K, there is

a large decrease in the electrical conductivity from 6000 Scm^{-1} to 1800 Scm^{-1}. Across the same range, there is a decrease in thermal conductivity from 8 $Wm^{-1}K^{-1}$ to 5 $Wm^{-1}K^{-1}$ and a rise in the Seebeck coefficient from 80 μVK^{-1} to 190 μVK^{-1}. The effect is that the fall in electrical conductivity cancels out the rise in the Seebeck coefficient and fall in the thermal conductivity, so the *ZT* value increases almost linearly as temperature increases. Between 900 K and 1273 K, the electrical conductivity falls at a slower rate but still nearly halves, falling to 1000 Scm^{-1} from 1800 Scm^{-1}. However, at the same time the thermal conductivity plateaus, only decreasing from 5 $Wm^{-1}K^{-1}$ to 4 $Wm^{-1}K^{-1}$ between 900 K and 1273 K, and the Seebeck coefficient start to level off with a smaller increase from 190 μVK^{-1} to 230 μVK^{-1}. Again, the effect of this is that the fall in electrical conductivity is counteracted by the slight fall in thermal conductivity and rise in the Seebeck coefficient, meaning that again the figure of merit rises almost linearly with temperature. At the top end of the temperature range, the *ZT* value starts to flatten off. This is because the rate of increase of the Seebeck effect continues to fall, but by this point the electrical and thermal conductivities have almost completely plateaued. Consequently, the flattening of the Seebeck coefficient curve is mirrored in the *ZT* curve.

The other enhancement of FeNbSb, $Fe_{1.05}Nb_{0.75}Ti_{0.25}Sb$, performed as well as $FeNb_{0.88}Hf_{0.12}Sb$ between 850 K and 950 K. The high *ZT* levels could not be maintained, however, as the rate of increase of the Seebeck coefficient drops from 950 K onwards, only increasing from 200 μVK^{-1} to 210 μVK^{-1} between 950 K and 1273 K. The effect of this is that the Seebeck coefficient cannot compensate for the falling electrical conductivity and the *ZT* value plateaus. $Fe_{1.05}Nb_{0.75}Ti_{0.25}Sb$ still records a maximum *ZT* value of 1.31 at 1133 K and a maximum efficiency of 22.91% at 1273 K.

Fu et al. (2016) found comparable real test values to these computational results when titanium (Ti) doping was found to synergistically supply extra carriers. This gives an optimum power factor and causes strain field fluctuations and greater electron-phonon scattering, leading to a large reduction in k_L [44]. Furthermore, using a ball milling process, the grain size can be significantly reduced and grain boundaries can be introduced, causing an increase in low frequency phonon scattering. The creation of atomic-scale point defects can also be used to enhance high frequency scattering [47]. Together, these two methods create hierarchical phonon scattering centres that reduce the value of k_L further. Consequently, from 1000 K to 1273 K, the thermal conductivity of $Fe_{1.05}Nb_{0.75}T_{0.25}Sb$ does not exceed 4 $Wm^{-1}K^{-1}$, which is extremely low for a half-Heusler material.

This is another case where aspects other than achieving a high *ZT* value come to prominence. For large-scale applications, which many of the high-temperature applications listed in Table 1 are, low material cost is just as important as a high figure of merit. Hafnium (Hf) is an expensive resource, with a current market price of around $1000 USD per kg, compared to titanium (Ti), which costs around $17 USD per kg. Furthermore, titanium is the ninth most abundant element in the Earth's crust with an estimated crustal abundance of 5.65 × 103 milligrams per kilogram, which is approaching three orders of magnitude greater than that of hafnium [48].

$Yb_{13.82}Pr_{0.18}MnSb_{11}$ shows a significant improvement on $Yb_{14}MnSb_{11}$ with a maximum *ZT* of 1.28 and a maximum efficiency of 23.23% at 1273 K. It does not display a dip in *ZT* after 1200 K like $Yb_{14}MnSb_{11}$, as the introduction of the light rare earth element praseodymium (Pr) causes the peak in the Seebeck coefficient to be shifted to a temperature above 1273 K, consequently meaning the dip in *ZT* does not occur until a higher temperature. As the simulation did not test above 1273 K, it is not known at what temperature the Seebeck coefficient, and therefore the *ZT* value, will start to dip.

Neither SiGe—20% SiMo nor $Yb_{13.5}La_{0.5}ZnSb_{11}$ manage to achieve *ZT* values above 0.9, with maximum values of 0.88 at 1273 K and 0.77 at 1213 K, respectively. Although Li et al. (2019) found SiGe—20% SiMo performs almost 50% better than all other additions of SiMo to SiGe when it comes to electrical conductivity, the downfall of SiGe—20% SiMo is its high thermal conductivity over the entire temperature range [45]. It starts at 4.9 $Wm^{-1}K^{-1}$ at 273 K, only dropping below 4 $Wm^{-1}K^{-1}$ for the first time at 1100 K, and finishes at 3.9 $Wm^{-1}K^{-1}$ at 1273 K. Although $Yb_{13.5}La_{0.5}ZnSb_{11}$ does not perform the best here, the maximum *ZT* of 0.77 recorded for this material is almost six times greater than the maximum value of 0.13 recorded when testing $Yb_{14}ZnSb_{11}$. Kunz Wille et al. (2019)

comment that such a drastic rise in *ZT* from $Yb_{14}ZnSb_{11}$ to $Yb_{13.5}La_{0.5}ZnSb_{11}$ is surprising considering the La^{3+} ions are simply replacing the Yb^{3+} ions in the material and therefore would not be expected to drastically affect *ZT* [35]. Consequently, there is a suggestion that there is much more to learn in the field of complex thermoelectric materials, especially at the nanoscale, in order to achieve even greater *ZT* values. This is particularly true for high-temperature materials, where there has been considerably less research compared to low- and mid-temperature range materials.

5. Conclusions

This investigation has computationally evaluated the performance of a range of market standard thermoelectric materials, before evaluating the effect of enhancements made using nanotechnology techniques in order to achieve potentially industry-leading figure of merit values in some of the materials. Over the low-temperature range, bismuth telluride was the best performer of the market standard materials with a peak *ZT* value of 0.91. After the enhancements had been modelled, $Mg_{0.97}Zn_{0.03}Ag_{0.9}Sb_{0.95}$ recorded the best *ZT* value of 1.45 and efficiency of 10.96%. However, $Zn_{0.015}Bi_{0.46}Sb_{1.54}Te_{3.015}$ performed better over the first 120 K of the temperature range, so it was determined to be the most appropriate material for near room temperature applications if making a judgement on performance alone. Other factors though, such as the low cost and abundance of magnesium-based materials, mean they would be better suited than $Zn_{0.015}Bi_{0.46}Sb_{1.54}Te_{3.015}$ for many near room temperature applications. Across the mid-temperature range, $AgSbTe_2$ performed the best of all the market standard materials and its enhancement, $AgSbTe_{1.85}Se_{0.15}$, performed the best of the enhanced materials, with a highest *ZT* value of 2.08 across the 600 K range. $AgSbTe_2$ and $AgSbTe_{1.85}Se_{0.15}$ are not viable materials at temperatures above 673 K so can only be used for applications that operate at the lower end of the mid-temperature range. For the upper 200 K of the range, $PbBi_{0.002}Te$–15% Ag_2Te, with a maximum *ZT* of 2.04 and a maximum efficiency of 23.27%, recorded the best performance. At the high-temperature range, FeNbSb did not perform well, but once enhanced, $FeNb_{0.88}Hf_{0.12}Sb$ outperformed the other materials with a maximum *ZT* value of 1.49 and a maximum efficiency of 25.33% at 1273 K. However, $Fe_{1.05}Nb_{0.75}Ti_{0.25}Sb$ performed competitively, with a *ZT* of 1.31 and, when the low material cost of titanium is factored in, compared to the expensive hafnium $Fe_{1.05}Nb_{0.75}Ti_{0.25}Sb$ it becomes an attractive proposition for large-scale applications.

An application for $Mg_{0.97}Zn_{0.03}Ag_{0.9}Sb_{0.95}$ would be for use in devices such as computer laptops, mobile phones, TVs and radios, where waste heat from the battery is converted into electrical energy to power or cool the device, prolonging battery life. Applications for $AgSbTe_{1.85}Se_{0.15}$ and $PbBi_{0.002}Te$–15% Ag_2Te could be in thermo electric devices (TEDs) that convert waste heat from hot water pipes in buildings to power wireless sensing systems used to control the building's temperature and humidity. $Fe_{1.05}Nb_{0.75}Ti_{0.25}Sb$ could be used in factories, where waste heat from furnaces or boilers is turned into the means of powering large turbines, and for use in the aerospace industry in TEDs used to convert waste heat from the aeroplane's engine into electrical energy to power the cockpit, lighting and other electrical systems. $FeNb_{0.88}Hf_{0.12}Sb$ would perhaps be most suitable for lasers and other precision engineering applications where heat lost at the point of contact is collected and converted back to power the machine.

Author Contributions: Conceptualization, P.S. and Q.W.; methodology, P.S. and Q.W.; software, Q.W. and P.S.; validation, Q.W., and P.S.; formal analysis, P.S.; investigation, P.S.; resources, Q.W.; data curation, P.S.; writing—original draft preparation, P.S.; writing—review and editing, Q.W.; visualization, Q.W.; supervision, Q.W.; project administration, Q.W.; All authors have read and agreed to the published version of the manuscript.

Funding: This research received no external funding.

Conflicts of Interest: The authors declare no conflict of interests.

References

1. Tervo, J.; Manninen, A.; Ilola, R.; Hannu Hänninen, H. *State of the Art of Thermoelectric Materials Processing*; Julkaislia-Utgivare Publisher: Espoo, Finland, 2009.
2. Zheng, X.F.; Liu, C.X.; Yan, Y.Y.; Wang, Q. A review of thermoelectrics research—Recent developments and potentials for sustainable and renewable energy applications. *Renew. Sustain. Energy Rev.* **2014**, *32*, 486–503. [CrossRef]
3. John Burn-Murdoch, J. *Up in Smoke: How Efficient is Electricity Produced in the UK*; John Burn-Murdoch, The Guardian: London, UK, 2012.
4. Taylor, A.L.; Dessai, S.; de Bruine Bruin, W. Public perception of climate risk and adaptation in the UK: A review of the literature. *Clim. Risk Manag.* **2014**, *4*, 1–16. [CrossRef]
5. Twaha, S.; Zhu, J.; Yan, Y.; Li, B. A comprehensive review of thermoelectric technology: Materials, applications, modelling and performance improvement. *Renew. Sustain. Energy Rev.* **2016**, *65*, 698–726. [CrossRef]
6. Snyder, G.J.; Toberer, E.S. Complex thermoelectric materials. *Nat. Mater.* **2008**, *7*, 105–114. [CrossRef]
7. Xiao, C.; Li, K.; Zhang, J.J.; Tong, W.; Liu, Y.W.; Li, Z.; Huang, P.C.; Pan, B.C.; Su, H.B.; Xie, Y. Magnetic Ions in Wide Band Gap Semiconductor Nanocrystals for Optimized Thermoelectric Properties. *Mater. Horiz.* **2014**, *1*, 81–86. [CrossRef]
8. Szczech, J.R.; Higgins, J.M.; Jin, S. Enhancement of the thermoelectric properties in nanoscale and nanostructured materials. *J. Mater. Chem.* **2011**, *21*, 4037–4055. [CrossRef]
9. Freer, R.; Powell, A.V. Realising the potential of thermoelectric technology: A Roadmap. *J. Mater. Chem. C* **2020**, *8*, 441–463. [CrossRef]
10. Crane, D.; LaGrandeur, J.; Jovovic, V.; Ranalli, M.; Adldinger, M.; Poliquin, E.; Dean, J.; Kossakovski, D.; Mazar, B.; Maranville, C. TEG On-Vehicle Performance and Model Validation and What It Means for Further TEG Development. *J. Electron. Mater.* **2013**, *42*, 1582–1591. [CrossRef]
11. Shen, Z.G.; Tian, L.L.; Liu, X. Automotive exhaust thermoelectric generators: Current status, challenges and future prospects. *Energy Convers. Manag.* **2019**, *195*, 1138–1173. [CrossRef]
12. Gould, C.A.; Shammas, N.Y.A.; Grainger, S.; Taylor, I. Thermoelectric Power Generation Properties, Application and Novel TCAD Simulation. In Proceedings of the 14th European Conference on Power Electronics and Applications, Birmingham, UK, 30 August–1 September 2011; pp. 1–10.
13. Von Lukowicz, M.; Abbe, E.; Schmiel, T.; Tajmar, M. Thermoelectric Generators on Satellites—An Approach for Waste Heat Recovery in Space. *Energies* **2016**, *9*, 541. [CrossRef]
14. Dusastre, V. (Ed.) *Materials for Sustainable Energy: A Collection of Peer-reviewed Research and Review Articles*; Nature Publishing Group, World Scientific: Singapore, 2011.
15. Yang, X.X.; Dai, Z.H.; Zhao, Y.C.; Niu, W.C.; Liu, J.Y.; Meng, S. Pressure induced excellent thermoelectric behaviour in skutterudites $CoSb_3$ and $IrSb_3$. *Phys. Chem. Chem. Phys.* **2019**, *21*, 851–858. [CrossRef] [PubMed]
16. LaLonde, A.D.; Pei, Y.Z.; Wang, H.; Snyder, G.J. Lead telluride alloy thermoelectrics. *Materialstoday* **2011**, *14*, 526–532. [CrossRef]
17. Hu, Y.F.; Bux, S.K.; Grebenkempera, J.H.; Kauzlarich, S.M. The effect of light rare earth element substitution in $Yb_{14}MnSb_{11}$ on thermoelectric properties. *J. Mater. Chem. C* **2015**, *3*, 10566–10573. [CrossRef]
18. Chen, X.; Dai, W.; Wu, T.; Luo, W.; Yang, J.; Jiang, W.; Wang, L. Thin Film Thermoelectric Materials: Classification, Characterization, and Potential for Wearable Applications. *Coatings* **2018**, *8*, 244. [CrossRef]
19. LeBlanc, S. Thermoelectric generators: Linking material properties and systems engineering for waste heat recovery applications. *Sustain. Mater. Technol.* **2014**, *1*, 26–35. [CrossRef]
20. Tian, Z.T.; Lee, S.; Chen, G. A Comprehensive Review of Heat Transfer in Thermoelectric Materials and Devices. *Annu. Rev. Heat Transf.* **2014**. [CrossRef]
21. Dehkordi, A.M.; Zebarjadic, M.; He, J.; Tritt, T.M. Thermoelectric power factor: Enhancement mechanisms and strategies for higher performance thermoelectric materials. *Mater. Sci. Eng. R Rep.* **2015**, *97*, 1–22. [CrossRef]
22. Gong, J.J.; Hong, A.J.; Shuai, J.; Li, L.; Yan, Z.B.; Ren, Z.F.; Liu, J.M. Investigation of the bipolar effect in the thermoelectric material CaMg2Bi2 using a firstprinciples study. *Phys. Chem. Chem. Phys.* **2016**, *18*, 16566–16574. [CrossRef]

23. Fitriania, R.O.; Long, B.D.; Barma, M.C.; Riaz, M.; Sabri, F.M.; Said, S.M.; Saidur, R. A review on nanostructures of high-temperature thermoelectric materials for waste heat recovery. *Renew. Sustain. Energy Rev.* **2016**, *64*, 635–659. [CrossRef]
24. Hu, X.K.; Yamamoto, A.; Ohta, M.; Nishiate, H. Measurement and simulation of thermoelectric efficiency for single leg. *Rev. Sci. Instrum.* **2015**, *86*, 045103. [CrossRef]
25. Wang, Y.T.; Liu, W.; Fan, A.; Li, P. Performance Comparison between Series-Connected and Parallel-Connected Thermoelectric Generator Systems. *Appl. Mech. Mater.* **2013**, *325*, 327–331. [CrossRef]
26. Park, K.; Ahn, K.; Cha, J.; Lee, S.; In Chae, S.; Cho, S.P.; Ryee, S.; Im, J.; Lee, J.; Park, S.D.; et al. Extraordinary off- stoichiometric Bismuth Telluride for enhanced n-type thermoelectric power factor. *J. Am. Chem. Soc.* **2016**, *138*, 14458–14468. [CrossRef] [PubMed]
27. Tan, G.; Hao, S.; Hanus, R.C.; Zhang, X.; Anand, S.; Bailey, T.P.; Rettie, A.J.E.; Su, X.; Uher, C.; Dravid, V.P.; et al. High thermoelectric performance in SnTe–$AgSbTe_2$ alloys from lattice softening, giant phonon–vacancy scattering, and valence band convergence. *ACS Energy Lett.* **2018**, *3*, 705–712. [CrossRef]
28. Hong, M.; Chen, Z.G.; Yang, L.; Liao, Z.M.; Zou, Y.C.; Chen, Y.H.; Matsumura, S.; Zou, J. Achieving ZT > 2 in p—Type AgSbTe2−xSex alloys via exploring the extra light valence band and introducing dense stacking faults. *Adv. Energy Mater.* **2018**, *8*, 1702333. [CrossRef]
29. Tanusilp, S.A.; Kurosaki, K. Si-Based materials for thermoelectric applications. *Materials* **2019**, *12*, 1943. [CrossRef] [PubMed]
30. Liu, Z.H.; Mao, J.; Sui, J.H.; Ren, Z.F. High thermoelectric performance of α-MgAgSb for power generation. *Energy Environ. Sci.* **2018**, *11*, 23–44. [CrossRef]
31. Srinivasan, B.; Gellé, A.; Gucci, F.; Boussard-Pledel, C.; Fontaine, B.; Gautier, R.; Halet, J.F.; Reeceb, M.J.; Bureaua, B. Realizing a stable high thermoelectric ZT ~ 2 over a broad temperature range in Ge1−x−yGaxSbyTe via band engineering and hybrid flash-SPS processing. *Inorg. Chem. Front.* **2019**, *6*, 63–73. [CrossRef]
32. Liu, W.S.; Lukas, K.C.; McEnaney, K.; Lee, S.; Zhang, Q.; Opeil, C.P.; Chen, G.; Ren, Z.F. Studies on the Bi2Te3–Bi2Se3–Bi2S3 system for mid-temperature thermoelectric energy conversion. *Energy Environ. Sci.* **2013**, *6*, 552–560. [CrossRef]
33. Hong, M.; Chen, Z.G.; Zou, J. Fundamental and progress of Bi2Te3-based thermoelectric materials. *Chin. Phys. B* **2018**, *27*, 048403.
34. Liu, D.M.; Li, X.Z.; de Castro Borlido, P.M.; Botti, S.; Schmechel, R.; Rettenmayr, M. Anisotropic layered Bi_2Te_3- In_2Te_3 composites: Control of interface density for tuning of thermoelectric properties. *Sci. Rep.* **2017**, *7*, 43611. [CrossRef]
35. Matsuoka, K.; Okuhata, M.; Hatsuta, N.; Takashiri, M. Effect of composition on the properties of bismuth telluride thin films produced by galvanostatic electrodeposition. *Trans. Mater. Res. Soc. Jpn.* **2015**, *40*, 383–387. [CrossRef]
36. Diliberto, S.; Richoux, V.; Stein, N.; Boulanger, C. Influence of pulsed electrodeposition on stoichiometry and thermoelectric properties of bismuth telluride films. *Phys. Stat. Sol.* **2008**, *205*, 2340–2344. [CrossRef]
37. Di, L.; Sun, R.R.; Qin, X.Y. Improving thermoelectric properties of p-type Bi2Te3-based alloys by spark plasma sintering. *Prog. Nat. Sci. Mater. Int.* **2011**, *21*, 336–340.
38. Saleemi, M.; Toprak, M.; Li, S.H.; Johnsson, M.; Muhammed, M. Synthesis, processing, and thermoelectric properties of bulk nanostructured Bismuth Telluride (Bi_2Te_3). *J. Mater. Chem.* **2012**, *22*, 725–730. [CrossRef]
39. Yu, K.; Zhou, Y.; Liu, Y.; Liu, F.; Hu, L.; Ao, W.; Li, J.; Xie, H. Near-room-temperature thermoelectric materials and their application prospects in geothermal power generation. *Geomech. Geophys. Geo-Energy Geo-Resour.* **2020**, *6*, 12. [CrossRef]
40. Zheng, Y.Y.; Liu, C.Y.; Miao, L.; Li, C.; Huang, R.; Gao, J.; Wang, X.Y.; Chen, J.; Zhou, Y.; Nishibori, E. Extraordinary thermoelectric performance in MgAgSb alloy with ultralow thermal conductivity. *Nano Energy* **2019**, *59*, 311–320. [CrossRef]
41. Mao, J.; Liu, W.S.; Ren, Z.F. Carrier distribution in multi-band materials and its effect on thermoelectric properties. *J. Mater.* **2016**, *2*, 203–211. [CrossRef]
42. Lee, M.H.; Yun, J.H.; Kim, G.; Lee, J.E.; Park, S.; Reith, H.; Schierning, G.; Nielsch, K.; Ko, W.; Li, A.; et al. Synergetic enhancement of thermoelectric performance by selective charge anderson localization–delocalization transition in n-Type Bi-Doped PbTe/Ag_2Te nanocomposite. *ACS Nano* **2019**, *13*, 3806–3815. [CrossRef]

43. Goyal, G.K.; Mukherjee, S.; Mallik, R.C.; Vitta, S.; Samajdar, I.; Dasgupta, T. High thermoelectric performance in $Mg_2(Si_{0.3}Sn_{0.7})$ by enhanced phonon scattering. *ACS Appl. Energy Mater.* **2019**, *2*, 2129–2137. [CrossRef]
44. Bhardwaj, A.; Shukla, A.K.; Dhakate, S.R.; Misra, D.K. Graphene boosts thermoelectric performance of a Zintl phase compound. *RSC Adv.* **2015**, *5*, 11058. [CrossRef]
45. Bhardwaj, R.; Gahtori, B.; Johari, K.K.; Bathula, S.; Chauhan, N.S.; Vishwakarma, A.; Dhakate, S.R.; Auluck, S.; Dhar, A. Collective effect of Fe and Se to improve the thermoelectric performance of unfilled p-Type $CoSb_3$ Skutterudites. *ACS Appl. Energy Mater.* **2019**, *2*, 1067–1076. [CrossRef]
46. Fu, C.G.; Wu, H.J.; Liu, Y.T.; He, J.Q.; Zhao, X.B.; Zhu, T.J. Enhancing the figure of merit of heavy—Band thermoelectric materials through hierarchical phonon scattering. *Adv. Mater.* **2016**, *3*, 1600035. [CrossRef]
47. Li, Y.; Han, J.; Xiang, Q.; Zhang, C.; Li, J. Enhancing thermoelectric properties of p-type SiGe by SiMo addition. *J. Mater. Sci. Mater. Electron.* **2019**, *30*, 9163–9170. [CrossRef]
48. Wille, E.L.K.; Grewal, N.S.; Bux, S.K.; Kauzlarich, S.M. Seebeck and figure of merit enhancement by rare earth doping in $Yb_{14-x}RE_xZnSb_{11}$ (x = 0.5). *Materials* **2019**, *12*, 731. [CrossRef] [PubMed]